RSC Advances

PAPER

View Article Online
View Journal | View Issue



Cite this: *RSC Adv.*, 2024, **14**, 13342

# New multiple-layered 3D polymers showing aggregation-induced emission and polarization†

Sai Zhang, *[a] Qingkai Yuan[b] and Guigen Li *[b]

Received 20th March 2024
Accepted 18th April 2024

DOI: 10.1039/d4ra02128b

rsc.li/rsc-advances

An exceptional achiral and chiral multilayer 3D polymer has been created and controlled by uniform and distinct aromatic chromophore units that are multiply sandwiched by naphthyl berths. In order to put together this assembly, it was necessary to search for new catalytic Suzuki–Miyaura polycouplings among various catalytic systems, monomers, and catalysts. Gel Permeation Chromatography (GPC) was able to verify the presence of many framework layers. The resulting achiral and chiral polymers displayed notable optical characteristic.



## Introduction

In the polymer and material sciences, molecular design has proven crucial in discovering desirable physical, chemical, and biological characteristics.[1–4] This is especially relevant to the research of conductive polymers, one of the most prominent fields of study during the last 20 years.[5–8] The conjugation of monomeric connections by C–C double or triple bonds for delocalizing π-electrons *via* their backbones is the main reason for the characteristics of conductive polymers.[9,10] Through-space conjugation has become an attractive alternative to conventional bonding pathways for energy and charge transfers in polymers.[11] In the meantime, exhaustively creating monomeric structures for poly- or copolymerization has demonstrated the practicality of charge-transfer connections hybridizing σ, π-, and through-space connections.[3,4] These conjugated polymers demonstrated a variety of electronic and optoelectronic properties, such as aggregation-induced emission (AIE)/aggregation-enhanced emission (AEE), conduction, thermally activated delayed fluorescence, optical nonlinearity, bipolar charge transport, multichannel and photocatalysis.[12]

In recent years, a new chirality called multilayer 3D chirality observed in our laboratories is primarily caused by aromatic–aromatic interactions that stack and space the layers.[13] As opposed to traditional planar or helical skeletons, this chirality displays rotational stereoisomerism. It was the Group-Assisted Purification (GAP) chemistry[14] that led to our first multilayer 3D chirality[13a] in which dual Buchwald–Hartwig cross-coupling[15] played an important role.

Multilayer 3D chirality is a new type of chirality that differs from conventional planar and helical chirality in that the layers are not bridged together (a highly compacted chiral fold held together primarily by π-stacking interactions). This new chiral framework called a multi-layer organic framework (M-LOF), consists of three roughly parallel layers: an aromatic ring at the top, middle, and bottom. It also contains unique C2- and/or pseudo C2-symmetry.[13] The compounds exhibiting multi-layer 3D chirality have restricted rotation between the top and bottom layers. It is interesting to note that this multi-layer type framework exhibits aspects of both planar and axial chirality or rotational stereoisomerism. The discovery of multilayer 3D chirality is expected to give opportunities for research in the fields of asymmetric synthesis and catalysis, as well as have a significant influence on the chemical, medical, and material sciences in the future.

Afterward, we developed a more widespread C–C bonding bridge with chiral auxiliaries and catalysts controlling stereochemistry.[16] The aggregated and diluted chiral multi-layer 3D compounds showed intriguing fluorescence under UV irradiation.[16a] In 2020, we achieved the synthesis of polymers of structurally compacted triple-columned/multi-layered framework and relevant oligomers. We also conducted the aggregation-induced emission (AIE) features and computational study of these targets[17] (Fig. 1a). In 2021, we synthesized chiral triple-column/multi-layered 3D folding polymers, stacking at least seven layers by various aromatic bridges[18] (Fig. 1b). In the same year, we successfully generated several other chiral polymers that had both uniformed and differentiated aromatic bridges in the middle of two bridge columns[19] (Fig. 1b). Under specified wavelength irradiation, achiral and chiral polymers in this study demonstrate surprising fluorescence activity in solution form.

In this work, we would like to report the design and synthesis of new achiral and chiral multi-layer polymers by using different monomers by taking advantage of Suzuki–Miyaura cross-

[a]*School of Pharmacy, Continuous Flow Engineering Laboratory of National Petroleum and Chemical Industry, Changzhou University, Changzhou, Jiangsu 213164, China*
[b]*Department of Chemistry and Biochemistry, Texas Tech University, Lubbock, Texas, 79409-1061, USA. E-mail: Guigen.li@ttu.edu*

† Electronic supplementary information (ESI) available. See DOI: https://doi.org/10.1039/d4ra02128b

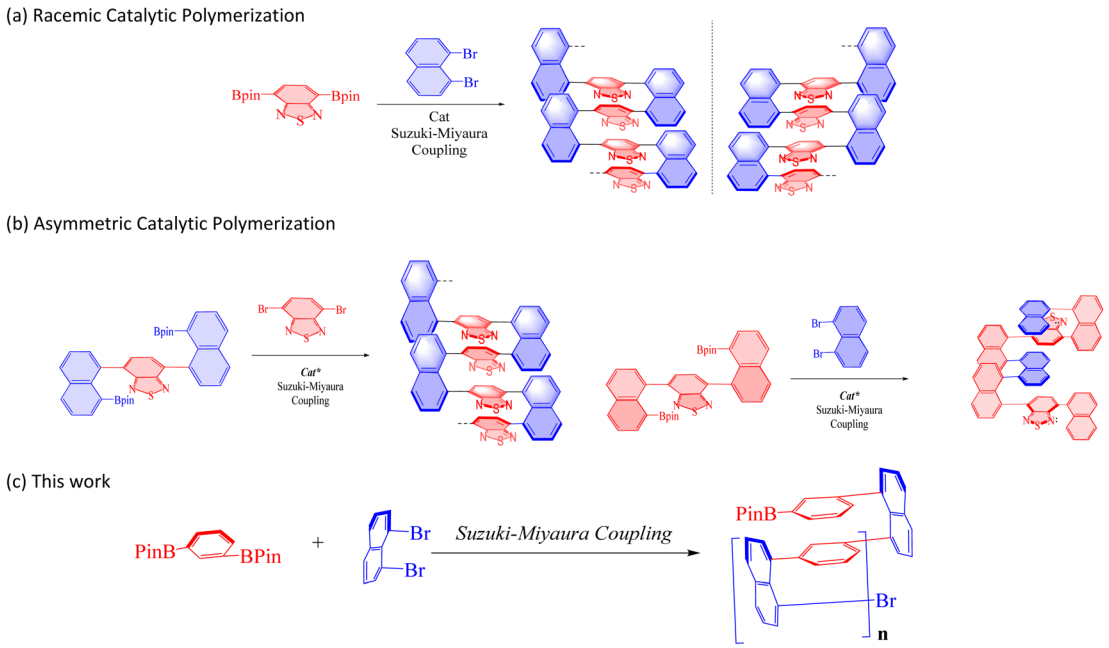


Fig. 1 (a) Formation of racemic polymers. (b) Asymmetric catalytic polymerization. Cat* represents chiral catalysts. (c) New multilayer 3D polymer.

coupling (Fig. 1c). We also reported their physical properties of UV-vis, photoluminescence (PL), Aggregation-Induced Emission (AIE), Aggregation-Induced Polarization[20] (AIP), CD spectroscopy, and SEM spectroscopy.

## Results and discussion

In our earlier design of multilayer 3D polymers, we used symmetrically or non-symmetrically substituted aromatic rings on their 1,4-position as bridges between column anchors.[18–20] In the current design, the bridges between column anchors in our earlier design of multi-layered 3D polymers were aromatic rings replaced symmetrically or non-symmetrically in their 1,3-position. In the current design, derivatives of 1,3-bis(4,4,5,5-tetramethyl-1,3,2-dioxaborolan-2-yl)benzene **1** scaffold, and derivatives of 1,8-dibromonaphthalene **4** were used as building blocks alternately. The resulting polymers in this work showed different arrangements of layered-column anchors than those in prior ones, in which a large distance existed between each pair of anchor planes. An additional naphthalene ring was put between each set of anchor planes, which is what caused this phenomenon. The Retro-Synthetic Analysis[21] (RSA) of **1A** was done by separating routes about two pairs of synthons to serve as a representative. Because it has been one of the most often used scaffolds in the fields of materials science and polymers, particularly in conductive polymers, synthon of benzene and naphthalene derivatives for the 1,3-coupling reaction was chosen as the starting material for this polymerization. The first route is the reaction by itself for 2-(3-(8-bromonaphthalen-1-yl) phenyl)-4,4,5,5-tetramethyl-1,3,2-dioxaborolane **1AA**, unfortunately the synthesis of 2-(3-(8-bromonaphthalen-1-yl)phenyl)-4,4,5,5-tetramethyl-1,3,2-dioxaborolane **1AA** is failed, and several previous attempts to create this synthesis is also failed. After that, we focused on the commercially available monomers of 1,8-dibromonaphthalene **4** and 5,6-dibromo-1,2-dihydroacenaphthylene **6**. Meanwhile, 1,8-dibromo-2,7-dimethoxynaphthalene 5 has a good yield in the process of synthesis.[22] In the same time, 1,3-bis(4,4,5,5-tetramethyl-1,3,2-dioxaborolan-2-yl)benzene **1**, 2,2′-(5-methoxy-1,3-phenylene) bis(4,4,5,5-tetramethyl-1,3,2-dioxaborolane) **2**, and 2,2′-(5-methyl-1,3-phenylene)bis(4,4,5,5-tetramethyl-1,3,2-dioxaborolane) **3**, which is easier to synthesize and has pretty good yield as the selected three monomer of boric acid ester[23] (Fig. 2 and 3). We screened a variety of mono- and bis-phosphine and Pd–ligand complexes using **1A** as the target to produce the desired polymer. Except for $Pd(PPh_3)_4$ and Pd(*S*-BINAP)$Cl_2$, the majority of the investigated achiral and chiral catalysts were unsuccessful.

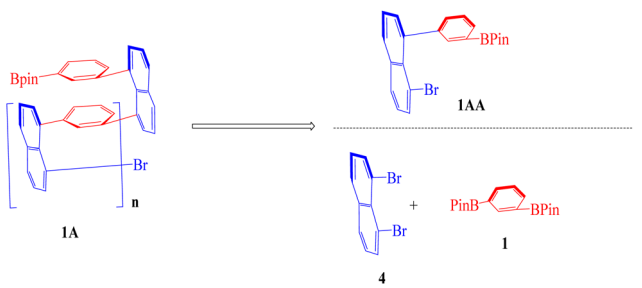


Fig. 2 Retro-Synthetic Analysis.

As shown in Scheme 1, five pairs of co-monomers **1–2**, and **4–6** were subjected to catalytic polymerization under multiple Suzuki–Miyaura cross-coupling systems. The synthesis of polymer **1A** was chosen as an example for description. A mol ratio of

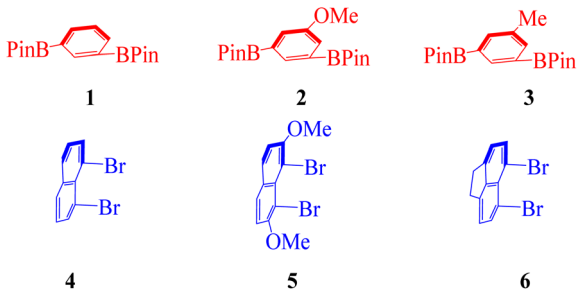


Fig. 3 Selected monomer.

1 : 1 of 1,8-dibromonaphthalene **4** to 1,3-bis(4,4,5,5-tetramethyl-1,3,2-dioxaborolan-2-yl)benzene **1** was mixed in THF/$H_2O$ (5 : 1, v/v) in the presence of $Pd(PPh_3)_4$ (5% mol) as the catalyst and potassium carbonate (3.0 equiv.) as an additive. The reaction was stirred at 88 °C for over 4 days until monomeric starting materials were consumed. The crude products were worked up by following standard procedure with nearly no small molecule impurities as revealed $^1$H-NMR analysis in DMSO-$d_6$ solvent. The solid was further dried to produce polymer **1A** as light-yellow solids (74% yield) (Scheme 2).

The synthetic and analytical results of six achiral polymers were summarized in Table 1. Polymers (**1A–2C**) were designed and synthesized by varying bridges and bridge piers (naphthyl columns) in chemical yields ranging from 38% to 82%. Gel permeation chromatography (GPC) was used to determine the molecular weights of polymers and oligomers in the solution of THF. Unlike our previous 1,4-substituted aromatic bridge polymers, the present 1,3-substituted aromatic bridge products exhibit better solubility of THF making GPC analysis more convenient. Among these six cases, **1A** afforded the highest $M_n$ and $M_w$, $M_w$ is 9792 and $M_n$ is 9427, respectively. However, cases **2A** and **2C** were generated as multilayer oligomers with layer numbers arranged from 7 to 9 based on the calculation of their

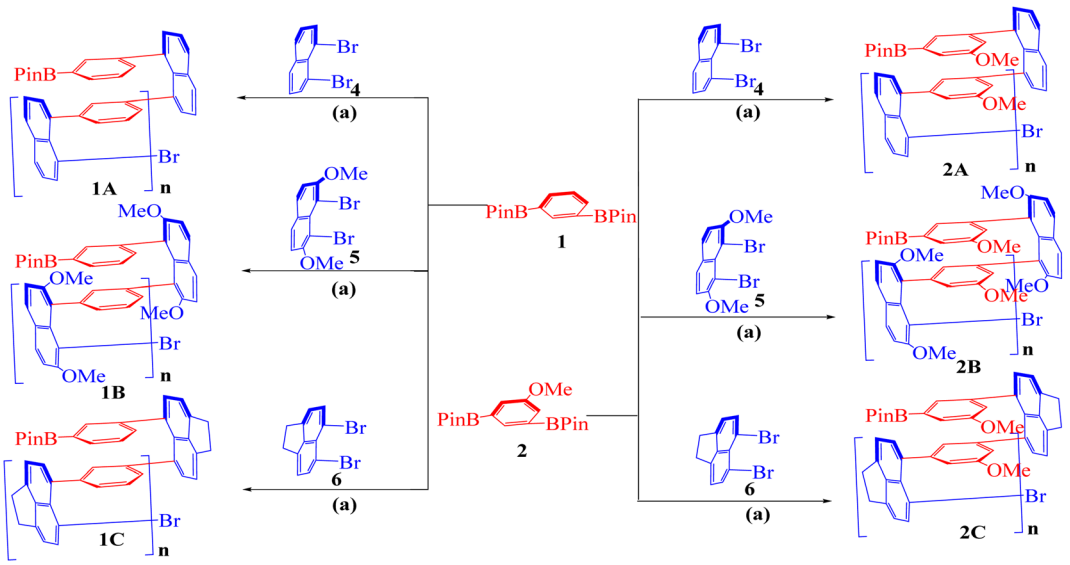


Scheme 1 (a) Multilayer polymer **1A–2C**. All reaction were carried out with substrates **1**, **2**, **4**, **5**, **6** (0.4 mmol), $Pd(PPh_3)_4$ (5 mol%) and $K_2CO_3$ in THF/$H_2O$ (10 : 2 mL) for 4 days under Ar.

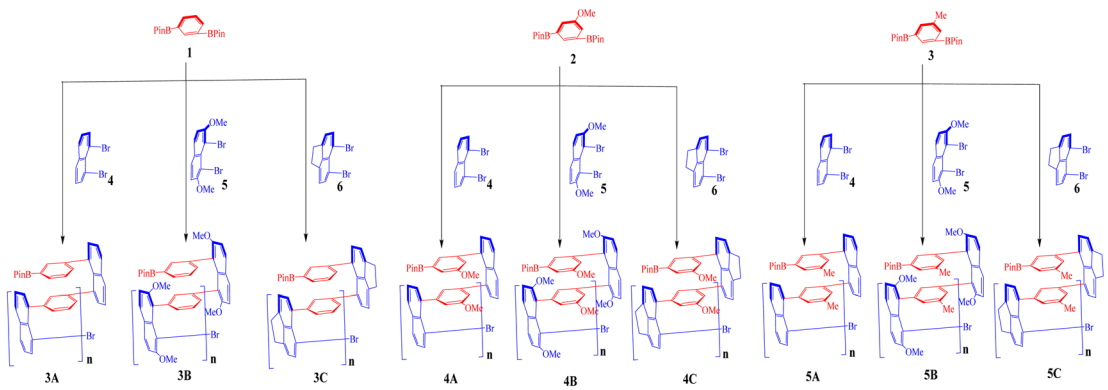


Scheme 2 Catalytic coupling assembly of multi-layer folding 3D chiral polymers **3A–5C**. All reactions were carried out with **1**, **2** and **3** (0.4 mmol), **4**, **5** or **6** (0.4 mmol), Pd(*S*-BINAP)$Cl_2$ (5 mol%) and $K_2CO_3$ (0.8 mmol) in THF/$H_2O$ (10 mL/2 mL) for 4 days under Argon protection.

Table 1 Results of synthetic racemic polymer and oligomer

| Poly-prod | Yield[a] [%] | $M_w$[b] | $M_n$[b] | PDI[c] | Theor. layers[d] |
|---|---|---|---|---|---|
| **1A** | 74 | 9792 | 9427 | 1.039 | 45 |
| **1B** | 81 | 8808 | 8318 | 1.059 | 30 |
| **1C** | 63 | 9226 | 8847 | 1.043 | 37 |
| **2A** | 81 | 2576 | 1885 | 1.366 | 7 |
| **2B** | 82 | 8086 | 7216 | 1.121 | 24 |
| **2C** | 38 | 2916 | 2629 | 1.109 | 9 |

[a] Isolated yield based on a comonomer for each case (co-monomers' ratio = 1 : 1). [b] Determined by GPC with a polystyrene standard. [c] PDI = $M_w/M_n$. [d] Based on $M_n$ of GPC determination.

$M_n$ data. It is difficult to explain the differences in synthetic efficiencies because polymerization depends on several factors, such as electronic effect, stereo effect, solubility, and reactivity of co-monomers and polymeric products.

Regarding the chiral reaction conditions that we decided upon, which produced the first result of polymer **3A** with a chemical yield of 60% and an optical rotation of $[\alpha]_D^{20} = +4$. Nine pairs of co-monomers were evaluated, as shown in Table 2, demonstrating good substrate scope even if many other similar substrates had not been studied. Table 2 provides an overview of nine different chiral polymer types' synthetic and analytical data. All of them simultaneously showed exceptional THF solubility, which facilitated easy examination using gel permeation chromatography (GPC). The nine polymers made it possible to conduct GPC analysis without difficulty and displayed $M_w$ ranging from 54 189 to 116 905 and $M_n$ from 49 101 to 68 002. According to the calculation that depends on the $M_n$ value, the number of polymer layers can range from 164 to 297. This indicates that the packing process is carried out in a satisfactory process.

Fifteen polymers' UV-vis absorption spectra in chloroform (Fig. 4a and b) showed one primary maximum below 400 nm. For achiral polymer **1A–2C**, the strong absorption occurred between 280 and 350 nm. The significant absorption peak for chiral polymer **3A–5C** occurred later compared to *t* achiral polymer **1A–2C**, and most of them exhibit similar UV characteristics.

All achiral and chiral polymers have been measured by photoluminescence (PL) evaluation, polymer **1B**, **4B**, and **5C** were found to be the phenomenon of aggregation-induced emission[12a] (AIE). As described in Fig. 4c, the emission maximum of **1B** was steadily increased as the water fractions ($f_w$) varied from 0% to 50%, indicating molecular motion suppression by intermolecular packing of polymer matrixes, which is attributed to the existence of aggregation-induced emission (AIE). For the other five achiral polymers, there is no obvious AIE characteristic. It would be noted that for this special multi-layered polymeric framework, parallel intermolecular and intramolecular packing make the corresponding movements more complicated as compared with small molecules or routine non-layered polymers. The present AIE through the through-space steric interactions is believed to be consistent with earlier observations on multilayer polymers. In the meantime, chiral Polymer **4B** and **5C** are also selected for photoluminescence (PL) evaluation for the part of chiral polymer, and very fortunately the water fractions ($f_w$) in Fig. 4d increased from 0% to 40%, progressively increasing the emission maxima of **4B** (Fig. 5c). This evident alteration could be attributed to the intermolecular packing of the polymer matrix. In terms of another AIE, polymer **5C** is in a situation that is essentially identical to polymer **4B** (Fig. 5e). The corresponding luminescent color coordinates of **1B**, **4B**, and **5C** were evaluated based on photoluminescence spectra and plotted using the CIE 1931 chromaticity diagram (Fig. 4f). These coordinates are as follows: **1B** (0.158, 0.024), **2B** (0.186, 0.263), and **3C** (0.162, 0.181), they can vary in color according to the different substructures.

The widespread availability of low-cost polarimeters in asymmetric synthesis research facilities makes this kind of AIP investigation a breeze to carry out. In 2021, we demonstrated that there is a connection between optical rotations of tiny chiral compounds in the presence of a certain percentage of water in THF.[20] Typical aggregation co-solvent systems produced optical results. Amplification and correction of rotation are more commonly referred to as aggregation-induced polarization. The optical rotation of chiral aggregates of multilayered chiral folding oligomers and polymers with water in THF has also been established. The optical rotation amplification and adjustment caused by typical aggregation cosolvent systems was termed aggregation-induced polarization (AIP). This phenomenon was identified during the design and

Table 2 Results of synthetic chiral polymers and oligomers

| Poly-prod | Yield[a] [%] | $M_w$[b] | $M_n$[b] | PDI[c] | $[\alpha]_D^{20}$[d] | Theor. layers[e] |
|---|---|---|---|---|---|---|
| **3A** | 60 | 88 548 | 51 362 | 1.724 | +4($c = 0.1$) | 253 |
| **3B** | 52 | 116 905 | 65 599 | 1.782 | +4($c = 0.1$) | 247 |
| **3C** | 62 | 115 241 | 68 002 | 1.695 | +43($c = 0.1$) | 297 |
| **4A** | 47 | 105 730 | 66 765 | 1.450 | +8($c = 0.1$) | 286 |
| **4B** | 51 | 102 227 | 64 469 | 1.585 | +2($c = 0.1$) | 220 |
| **4C** | 44 | 77 682 | 49 209 | 1.579 | −12.5($c = 0.1$) | 189 |
| **5A** | 46 | 95 336 | 57 119 | 1.669 | −40($c = 0.1$) | 231 |
| **5B** | 72 | 70 448 | 50 202 | 1.403 | +3($c = 0.1$) | 181 |
| **5C** | 71 | 54 189 | 40 101 | 1.351 | −2($c = 0.1$) | 164 |

[a] Isolated yield based on substrate **3A–5C**. [b] Determined by GPC with a polystyrene standard. [c] PDI = $M_w/M_n$. [d] In THF; $c$ = g/100 mL. [e] Based on $M_n$ of GPC.

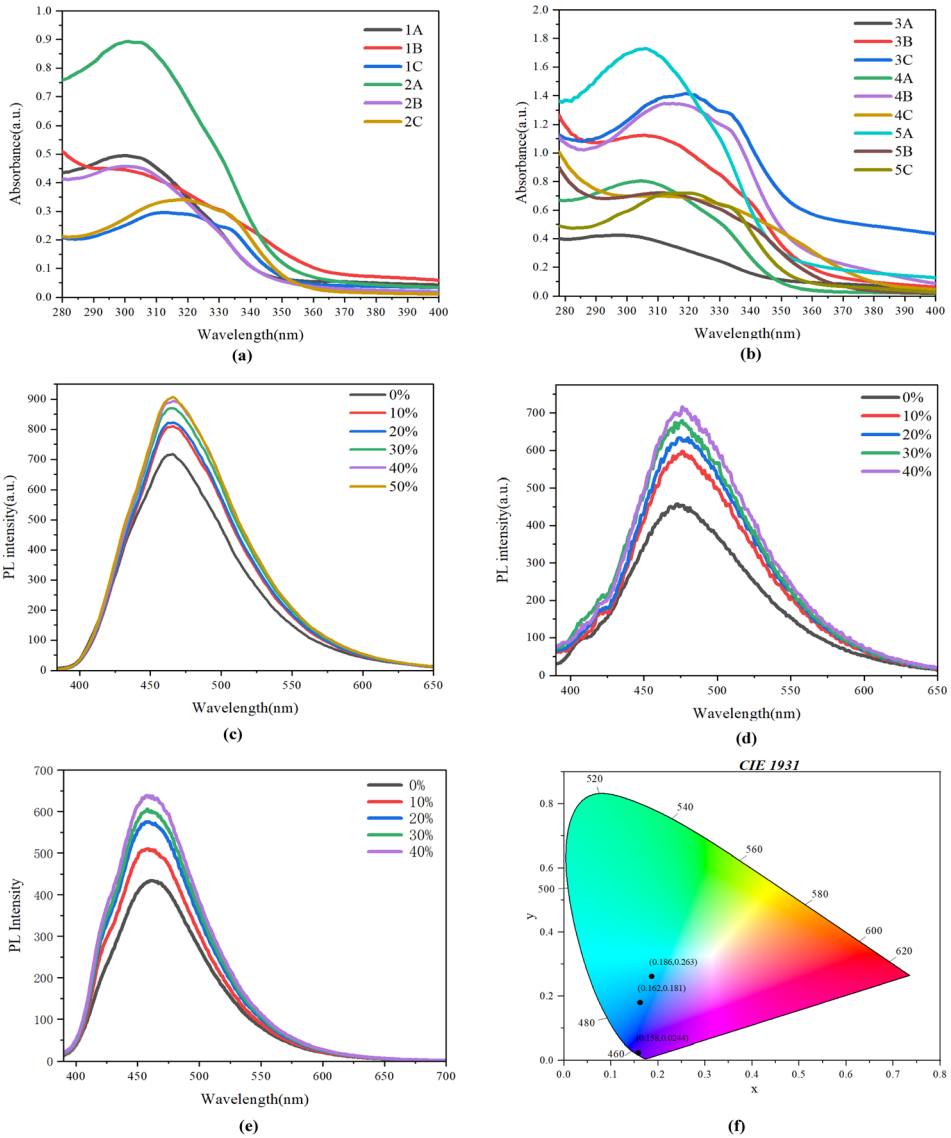


Fig. 4 (a) and (b) UV/vis absorption spectra of **1A–2C** and **3A–5C** in $CHCl_3$; $c = 0.05$ mg $mL^{-1}$. (c)–(e) PL spectra of **1B**, **4B** and **5C** in THF/water mixtures with different water fractions ($f_w$); $c = 0.05$ mg $mL^{-1}$; inset: fluorescence photographs of **1B**, **4B** & **5C** in THF/water system; (f) CIE 1931 chromaticity diagram of **1B**, **4B** and **5C** in THF.

synthesis of new multilayered chiral oligomers/polymers and was later discovered to exist in triple-column/multiple-layer chiral folding polymer THF-$H_2O$ systems. Here, we report the acquisition of optical rotation data of chiral polymers and oligomers at roughly room temperature using a sodium lamp and a Rudolph polarimeter (Rudolph Research Analytical APIV/2W). The concentrations of THF and its cosolvents ($c$ = 1 mg $L^{-1}$, 0.5 mg $mL^{-1}$, or 0.4 mg $mL^{-1}$) used in the measurements were all taken in a 2 mL vessel. The optical rotation data indicated some instability for most solutions in this investigation after the fraction of water ($f_w$) exceeded 30%; this is likely due to the increased glass surface tension near the vessel's extremities.

For this measurement, the water fraction, denoted by "$f_w$" was established at the component of 5% (v/v) on the X-horizontal coordinate, which corresponded to a certain rotation on the Y-vertical ordinate. We convincingly discovered that these polymers likewise exhibited discernible AIP effects, even if the resultant relationship curves had various forms. In the investigation of polymer **3B**, the optical rotation was initiated with positive data of 2.0° in THF in the absence of water ($f_w$ = 0%), but these data turned out to be higher when the amount of water present was increased to 5%, after that, the good results continued until the percentage of water reached 30% when the fractional weight was increased from 25% to 30%, we saw an enormous spike. Additionally, polymer **4C** demonstrated an overall improvement in optical rotation, there was a significant rise in the amount of leap when the fractional weight reached 20%. When the fractional weight of polymer **5B** was raised to 30%, there was a large rise followed by a little declining trend

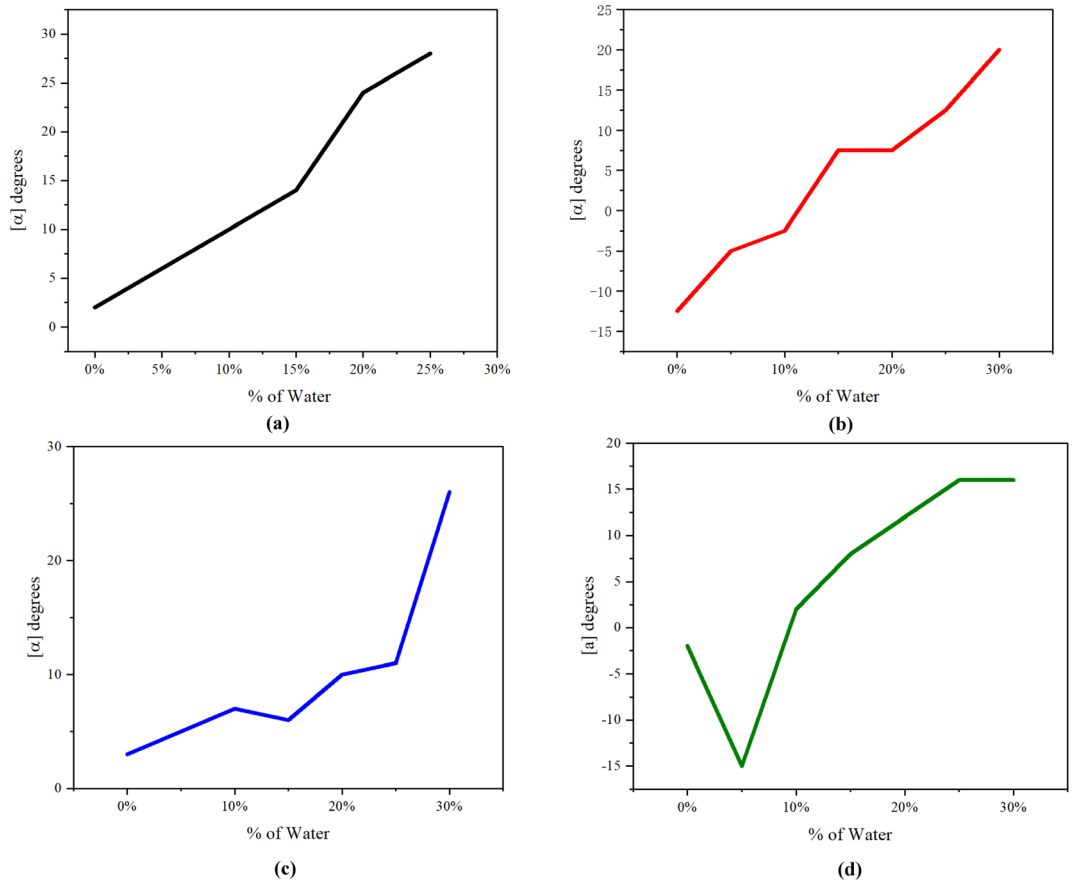


Fig. 5 Aggregation-induced polarization (AIP) of new multilayer 3D chirality oligomers. (a) AIP of chiral folding polymer **3B** in THF; $c = 0.5$ mg mL$^{-1}$. (b) AIP of chiral folding polymer **4C** in THF; $c = 0.4$ mg mL$^{-1}$. (c) AIP of chiral folding polymer **5B** in THF; $c = 1$ mg mL$^{-1}$. (d) AIP of chiral folding polymer **5C** in THF; $c = 0.5$ mg mL$^{-1}$.

between the ranges of 15% and 20%. Polymer **5C** first exhibited a negative optical rotation of −2°, which then precipitously decreased to −15° after the water percentage was raised to 5%, when the fractional weight reached 30%, the optical rotation was reversed and reset to 16°, and between 5% and 30%, there is a tendency toward rising proportions.

It is quite challenging to offer a mechanical explanation at this early stage for any of the situations that were investigated as part of this AIP effort. The fact that multilayer chiral oligomers and polymers exist as complexes of varying aggregation sizes was the root cause of the complication that arose from the scenario. To the best of our knowledge, there has not been any direct association between optical rotation and structures of complex mixes documented in the literature so far. This is due to a lack of empirical data that would allow for more in-depth research of the AIP process. In the future, it will be important to do further research in the fields of molecular design, computational organic chemistry, and physical organic chemistry.

CD spectroscopies were used to conduct additional investigations into the optical activities of certain chiral polymers **3A** and **3B** that were dissolved in methanol. The π–π* transition of aromatic rings accounted for the only optical absorption that was observed between 210 and 250 nm. Polymer **3A** displayed strong Cotton effects in the ranges of 211–215 nm, 218–220 nm, 223–225 nm, 226–227 nm, and 243–245 nm, as shown in Fig. 6. On the other hand, it exhibited strong Cotton effects in the ranges of 215–218 nm, 220–223 nm, 225–227 nm, 227–230 nm,

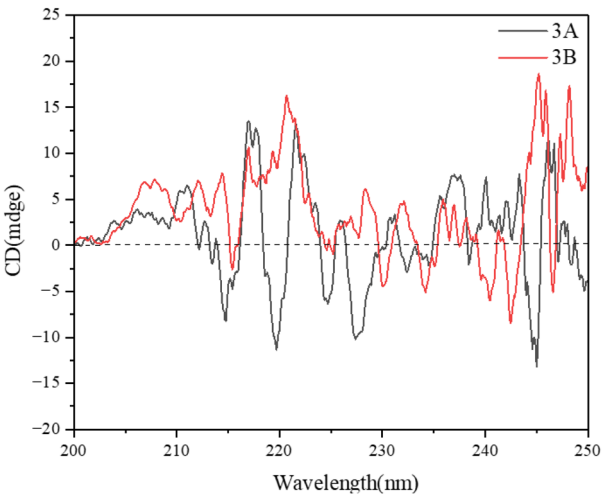


Fig. 6 CD spectra of **3A** & **3B** in methanol; $c = 0.2$ mg mL$^{-1}$.

and 243–245 nm. For polymer **3B**, an irregular chiral environment of the polymer backbone can be observed, this chiral environment has Cotton effects that are negative and are centered at approximately 210 nm and 250 nm. The other seven chiral polymers, **3C**, **4A**, **4B**, **4C**, **5A**, **5B**, and **5C**, are extremely hard to dissolve in methanol solvent, and examining them with CD spectroscopies reveals that there is no noticeable cotton effect.

SEM imaging is utilized rather commonly in biopolymer and composite films to evaluate the surface topography, homogeneity, and any phase separation that may occur between the various components. To explore the morphology of chiral folding polymers and achiral polymers, scanning electron microscopy (SEM) was utilized. Solid polymer samples were given a coating of a very thin layer of gold so that the conductivity could be increased, and the signal-to-noise ratio could be decreased. In the achiral polymer **1A**, there were a lot of spherical aggregates that were the same material, but they were varied sizes. The particle for polymer **2B** has a stronger concentration that is noticeably higher in comparison to polymer **1A** (Fig. 7).

Chiral polymers are more fragmented than achiral polymers as shown in Fig. 8a and b show that particles of various sizes aggregate layer by layer. This surface phenomenon corresponds to the ideal assumption of molecular aggregation, and the gaps between the particles are relatively small. The particle in polymer **5C**, which exhibits AIE characteristics, the particle's gap is significantly larger than those of the other three chiral polymers (**3C**, **4C**, and **5A**), but there is also a noticeable gap between the larger particles (Fig. 8). This indicates that the dispersed spatial phenomena can be related to the polymer's intriguing AIE characteristics.

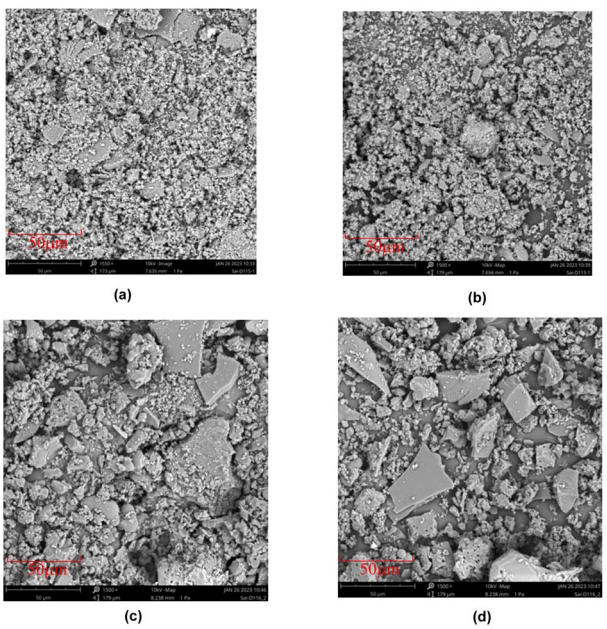


Fig. 7 SEM images of selected achiral polymers **1A** (top) and **2B** (bottom).

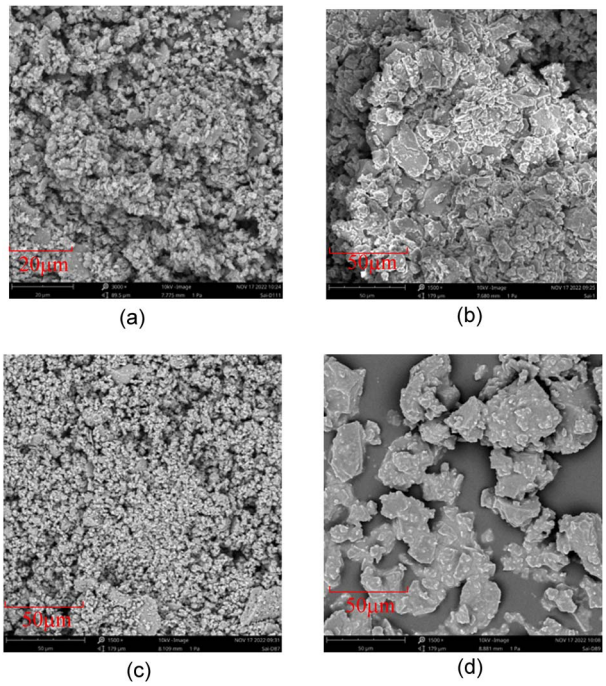


Fig. 8 SEM of chiral folding polymers (a) **3C**, (b)**4C**, (c)**5A**, (d) **5C**.

## Conclusions

In conclusion, we were able to successfully synthesize twelve achiral and chiral multilayer 3D polymers with multiple layers and triple columns, stacking up between 7 layers and 297 layers by different aromatic bridges under achiral and chiral catalytic condition. UV, optical rotation, AIE, and AIP characteristics express their applicational potentials, SEM images of selected newly discovered achiral and chiral polymers have been obtained, revealing good conductivity and positive. Cotton effects as well as cauliflower-like formations on their surfaces, each of them bears non-uniform distribution of homogenous balls. Multilayer 3D chirality has made considerable progress in recent years[16b,24] and brought out orientational chirality,[25] new aggregation-induced phenomenon[26](AIS, AIC), but there is still a long way to go for practical application. This discovery will bring new opportunities for the development of multilayer 3D materials in the future, further investigation of new 3D multilayer polymer which has AIE characteristics on variation of chromaticity, and fluorescence bioimaging of cancer cells will be conducted in due course.

## Author contributions

SZ: writing original draft and investigation. QY: writing original draft and measuring UV and fluorescence data. GL: supervising and writing original draft.

## Conflicts of interest

There are no conflicts to declare.

## Acknowledgements

We would like to acknowledge the financial support from Robert A. Welch Foundation (D1361-20210327, USA), and the National Natural Science Foundation of China (22071102 and 91956110).

## Notes and references

1 T. A. Skotheim, *Handbook of Conducting Polymers: Volume 1: in Two Volumes, Marcel Dekker*, New York, NY, 1986.
2 (*a*) D. J. Hill, M. J. Mio, R. B. Prince, T. S. Hughes and J. S. Moore, *Chem. Rev.*, 2001, **101**, 3893–4012; (*b*) K. Oh, K. S. Jeong and J. S. Moore, *Nature*, 2001, **414**, 889–893.
3 (*a*) S. W. Thomas 3rd, G. D. Joly and T. M. Swager, *Chem. Rev.*, 2007, **107**, 1339–1386; (*b*) A. J. Varni, A. Fortney, M. A. Baker, J. C. Worch, Y. Qiu, D. Yaron, S. Bernhard, K. J. T. Noonan and T. Kowalewski, *J. Am. Chem. Soc.*, 2019, **141**, 8858–8867.
4 (*a*) S. H. Gellman, *Acc. Chem. Res.*, 1998, **31**, 173–180; (*b*) J. M. Tour, *Acc. Chem. Res.*, 2000, **33**, 791–804; (*c*) J. M. Tour, *Chem. Rev.*, 1996, **96**, 537–554.
5 *Nonlinear Optical Effects in Organic Polymers*, ed. J. Messier, P. Prasad and D. Ulrich, Springer, New York, NY, 2014.
6 T. Nakano, *Polym. J.*, 2010, **42**, 103–123.
7 (*a*) J. Li, P. Shen, Z. Zhao and B. Z. Tang, *CCS Chem.*, 2019, **1**, 181–196; (*b*) G. Niu, X. Zheng, Z. Zhao, H. Zhang, J. Wang, X. He, Y. Chen, X. Shi, C. Ma, R. T. K. Kwok, J. W. Y. Lam, H. H. Y. Sung, I. D. Williams, K. S. Wong, P. Wang and B. Z. Tang, *J. Am. Chem. Soc.*, 2019, **141**, 15111–15120; (*c*) L. Xu, Z. Wang, R. Wang, L. Wang, X. He, H. Jiang, H. Tang, D. Cao and B. Z. Tang, *Angew Chem. Int. Ed. Engl.*, 2020, **59**, 9908–9913.
8 R. Gutzler and D. F. Perepichka, *J. Am. Chem. Soc.*, 2013, **135**, 16585–16594.
9 H. Shirakawa, E. J. Louis, A. G. MacDiarmid, C. K. Chiang and A. J. Heeger, *J. Chem. Soc. Chem. Commun.*, 1977, 578.
10 N. Hall, *Chem. Commun.*, 2003, 1–4.
11 Z. Lian, J. He, L. Liu, Y. Fan, X. Chen and H. Jiang, *Nat. Commun.*, 2023, **14**, 2752.
12 (*a*) H. Wang, Q. Li, P. Alam, H. Bai, V. Bhalla, M. R. Bryce, M. Cao, C. Chen, S. Chen, X. Chen, Y. Chen, Z. Chen, D. Dang, D. Ding, S. Ding, Y. Duo, M. Gao, W. He, X. He, X. Hong, Y. Hong, J.-J. Hu, R. Hu, X. Huang, T. D. James, X. Jiang, G.-I. Konishi, R. T. K. Kwok, J. W. Y. Lam, C. Li, H. Li, K. Li, N. Li, W.-J. Li, Y. Li, X.-J. Liang, Y. Liang, B. Liu, G. Liu, X. Liu, X. Lou, X.-Y. Lou, L. Luo, P. R. McGonigal, Z.-W. Mao, G. Niu, T. C. Owyong, A. Pucci, J. Qian, A. Qin, Z. Qiu, A. L. Rogach, B. Situ, K. Tanaka, Y. Tang, B. Wang, D. Wang, J. Wang, W. Wang, W.-X. Wang, W.-J. Wang, X. Wang, Y.-F. Wang, S. Wu, Y. Wu, Y. Xiong, R. Xu, C. Yan, S. Yan, H.-B. Yang, L.-L. Yang, M. Yang, Y.-W. Yang, J. Yoon, S.-Q. Zang, J. Zhang, P. Zhang, T. Zhang, X. Zhang, X. Zhang, N. Zhao, Z. Zhao, J. Zheng, L. Zheng, Z. Zheng, M.-Q. Zhu, W.-H. Zhu, H. Zou and B. Z. Tang, *ACS Nano*, 2023, **17**, 14347–14405; (*b*) J. Wang, J. Mei, E. Zhao, Z. Song, A. Qin, J. Z. Sun and B. Z. Tang, *Macromolecules*, 2012, **45**, 7692–7703; (*c*) F. Ni, J. Zhang, Y. Zhou and L. Qiu, *Chem Catal.*, 2024, 100915.
13 (*a*) G. Wu, Y. Liu, Z. Yang, N. Katakam, H. Rouh, S. Ahmed, D. Unruh, K. Surowiec and G. Li, *Research*, 2019, **2019**, 6717104; (*b*) G. Wu, Y. Liu, Z. Yang, T. Jiang, N. Katakam, H. Rouh, L. Ma, Y. Tang, S. Ahmed, A. U. Rahman, H. Huang, D. Unruh and G. Li, *Natl. Sci. Rev.*, 2020, **7**, 588–599; (*c*) J. Zhang and L. Kürti, *Natl. Sci. Rev.*, 2021, **8**, nwaa205; (*d*) Y. Liu, G. Wu, Z. Yang, H. Rouh, N. Katakam, S. Ahmed, D. Unruh, Z. Cui, H. Lischka and G. Li, *Sci. China: Chem.*, 2020, **63**, 692–698.
14 (*a*) G. An, C. Seifert and G. Li, *Org. Biomol. Chem.*, 2015, **13**, 1600–1617; (*b*) A. U. Rahman, N. Zarshad, I. Khan, F. Faiz, G. Li and A. Ali, *Front. Chem.*, 2021, **9**, DOI: **10.3389/fchem.2021.742399**; (*c*) A. U. Rahman, N. Zarshad, P. Zhou, W. Yang, G. Li and A. Ali, *Front. Chem.*, 2020, **8**, DOI: **10.3389/fchem.2020.00523**.
15 (*a*) P. A. Forero-Cortés and A. M. Haydl, *Org. Process Res. Dev.*, 2019, **23**, 1478–1483; (*b*) M. M. Heravi, Z. Kheilkordi, V. Zadsirjan, M. Heydari and M. Malmir, *J. Organomet. Chem.*, 2018, **861**, 17–104.
16 (*a*) G. Wu, Y. Liu, H. Rouh, L. Ma, Y. Tang, S. Zhang, P. Zhou, J.-Y. Wang, S. Jin, D. Unruh, K. Surowiec, Y. Ma and G. Li, *Chem.–Eur. J.*, 2021, **27**, 7977; (*b*) Y. Liu, H. Rouh, Y. Tang, G. Wu, Q. Yuan, S. Zhang, J.-Y. Wang, S. Jin, T. Xu, Y. Wang, J. Pan, D. Unruh and G. Li, *Synlett*, 2023, **34**, 153–158.
17 G. Wu, Y. Liu, Z. Yang, L. Ma, Y. Tang, X. Zhao, H. Rouh, Q. Zheng, P. Zhou, J.-Y. Wang, F. Siddique, S. Zhang, S. Jin, D. Unruh, A. J. A. Aquino, H. Lischka, K. M. Hutchins and G. Li, *Research*, 2021, **2021**, DOI: **10.34133/2021/3565791**.
18 J.-Y. Wang, Y. Tang, G.-Z. Wu, S. Zhang, H. Rouh, S. Jin, T. Xu, Y. Wang, D. Unruh, K. Surowiec, Y. Ma, Y. Li, C. Katz, H. Liang, W. Cong and G. Li, *Chem.–Eur. J.*, 2022, **28**, e202104102.
19 Y. Tang, S. Jin, S. Zhang, G.-Z. Wu, J.-Y. Wang, T. Xu, Y. Wang, D. Unruh, K. Surowiec, Y. Ma, S. Wang, C. Katz, H. Liang, Y. Li, W. Cong and G. Li, *Research*, 2022, **2022**, DOI: **10.34133/2022/9847949**.
20 (*a*) Y. Tang, S. Zhang, T. Xu, Q. Yuan, J.-Y. Wang, S. Jin, Y. Wang, J. Pan, I. Griffin, D. Chen and G. Li, *Front. Chem.*, 2022, **10**, 962638; (*b*) Y. Tang, Q. Yuan, Y. Wang, S. Zhang, J.-Y. Wang, S. Jin, T. Xu, J. Pan, C. R. Guilbeau, A. J. Pleasant and G. Li, *RSC Adv.*, 2022, **12**, 29813–29817.
21 E. J. Corey and X.-M. Cheng, *The Logic of Chemical Synthesis*, Wiley-Interscience, New York, 2009.
22 R. S. Grainger, B. Patel, B. M. Kariuki, L. Male and N. Spencer, *J. Am. Chem. Soc.*, 2011, **133**, 5843–5852.
23 (*a*) J. Tasseroul, M. M. Lorenzo-Garcia, J. Dosso, F. Simon, S. Velari, A. De Vita, P. Tecilla and D. Bonifazi, *J. Org. Chem.*, 2020, **85**, 3454–3464; (*b*) A. M. Antonio, M. R. Dworzak, K. J. Korman, G. P. A. Yap and E. D. Bloch, *Chem. Mater.*, 2022, **34**, 10823–10831.
24 (*a*) Y. Tang, G. Wu, S. Jin, Y. Liu, L. Ma, S. Zhang, H. Rouh, A. I. M. Ali, J.-Y. Wang, T. Xu, D. Unruh, K. Surowiec and G. Li, *J. Org. Chem.*, 2022, **87**, 5976–5986; (*b*) S. Jin,

J.-Y. Wang, Y. Tang, H. Rouh, S. Zhang, T. Xu, Y. Wang, Q. Yuan, D. Chen, D. Unruh and G. Li, *Front. Chem.*, 2022, **10**, DOI: **10.3389/fchem.2022.860398**; (*c*) S. Zhang, D. Chen, J.-Y. Wang, S. Yan and G. Li, *Front. Chem.*, 2023, **11**, DOI: **10.3389/fchem.2023.1259609**; (*d*) Y. Tang, Q. Yuan, S. Zhang, J.-Y. Wang, K. Surowiec and G. Li, *RSC Adv.*, 2024, **14**, 2792–2795.

25 (*a*) S. Jin, Y. Wang, Y. Tang, J.-Y. Wang, T. Xu, J. Pan, S. Zhang, Q. Yuan, A. U. Rahman, J. D. McDonald, G.-Q. Wang, S. Li and G. Li, *Research*, 2022, **2022**, DOI: **10.34133/research.0012**; (*b*) S. Jin, T. Xu, Y. Tang, J.-Y. Wang, Y. Wang, J. Pan, S. Zhang, Q. Yuan, A. U. Rahman, A. J. A. Aquino, H. Lischka and G. Li, *Front. Chem.*, 2022, **10**, 1110240; (*c*) Y. Wang, T. Xu, S. Jin, J.-Y. Wang, Q. Yuan, H. Liu, Y. Tang, S. Zhang and G. Li, *Chem.–Eur. J.*, 2024, e202400005, DOI: **10.1002/chem.202400005**.

26 (*a*) H. Rouh, Y. Tang, T. Xu, Q. Yuan, S. Zhang, J.-Y. Wang, S. Jin, Y. Wang, J. Pan, H. L. Wood, J. D. McDonald and G. Li, *Research*, 2022, **2022**, 9865108; (*b*) Y. Tang, Y. Wang, Q. Yuan, S. Zhang, J.-Y. Wang, S. Jin, T. Xu, J. Pan, K. Surowiec and G. Li, *Research*, 2023, DOI: **10.34133/research.0163**.